



UNIVERSITY OF LEEDS

This is a repository copy of *Mechanism of tribofilm formation on Ti6Al4V oxygen diffusion layer in a simulated body fluid*.

White Rose Research Online URL for this paper:

<http://eprints.whiterose.ac.uk/122831/>

Version: Accepted Version

---

**Article:**

Yazdi, R, Ghasemi, HM, Abedini, M et al. (2 more authors) (2018) Mechanism of tribofilm formation on Ti6Al4V oxygen diffusion layer in a simulated body fluid. *Journal of the Mechanical Behavior of Biomedical Materials*, 77. pp. 660-670. ISSN 1751-6161

<https://doi.org/10.1016/j.jmbbm.2017.10.020>

---

© 2017 Elsevier Ltd. This is an author produced version of a paper published in *Journal of the Mechanical Behavior of Biomedical Materials*. Uploaded in accordance with the publisher's self-archiving policy. This manuscript version is made available under the CC-BY-NC-ND 4.0 license <http://creativecommons.org/licenses/by-nc-nd/4.0/>

**Reuse**

Items deposited in White Rose Research Online are protected by copyright, with all rights reserved unless indicated otherwise. They may be downloaded and/or printed for private study, or other acts as permitted by national copyright laws. The publisher or other rights holders may allow further reproduction and re-use of the full text version. This is indicated by the licence information on the White Rose Research Online record for the item.

**Takedown**

If you consider content in White Rose Research Online to be in breach of UK law, please notify us by emailing [eprints@whiterose.ac.uk](mailto:eprints@whiterose.ac.uk) including the URL of the record and the reason for the withdrawal request.

# Author's Accepted Manuscript

Mechanism of tribofilm formation on Ti6Al4V oxygen diffusion layer in a simulated body fluid

R. Yazdi, H.M. Ghasemi, M. Abedini, C. Wang,  
A. Neville



PII: S1751-6161(17)30447-2

DOI: <https://doi.org/10.1016/j.jmmbm.2017.10.020>

Reference: JMBBM2540

To appear in: *Journal of the Mechanical Behavior of Biomedical Materials*

Received date: 30 August 2017

Revised date: 10 October 2017

Accepted date: 15 October 2017

Cite this article as: R. Yazdi, H.M. Ghasemi, M. Abedini, C. Wang and A. Neville, Mechanism of tribofilm formation on Ti6Al4V oxygen diffusion layer in a simulated body fluid, *Journal of the Mechanical Behavior of Biomedical Materials*, <https://doi.org/10.1016/j.jmmbm.2017.10.020>

This is a PDF file of an unedited manuscript that has been accepted for publication. As a service to our customers we are providing this early version of the manuscript. The manuscript will undergo copyediting, typesetting, and review of the resulting galley proof before it is published in its final citable form. Please note that during the production process errors may be discovered which could affect the content, and all legal disclaimers that apply to the journal pertain.

## Mechanism of tribofilm formation on Ti6Al4V oxygen diffusion layer in a simulated body fluid

**R. Yazdi<sup>a</sup>, H.M. Ghasemi<sup>a\*</sup>, M. Abedini<sup>b</sup>, C. Wang<sup>c</sup>, A. Neville<sup>c</sup>**

a: School of Metallurgy and Materials Engineering, College of Engineering, University of Tehran, Tehran, Iran

b: Department of Metallurgy and Materials Engineering, Faculty of Engineering, University of Kashan, Kashan, Iran

c: Institute of Functional Surfaces, School of Mechanical Engineering, University of Leeds, Leeds, LS2 9JT, UK

\*Corresponding author. Tel: +98 2161114095, E-mail address: hghasemi@ut.ac.ir (H.M. Ghasemi).

### Abstract

An Oxygen Diffusion Layer (ODL) was generated on the surface of Ti6Al4V alloy by thermal oxidation treatment. In vitro tests for cytotoxicity were performed in the presence of Ti6Al4V and the ODL samples with the culture of G292 Cells and using MTT assay. The results showed a similar cell viability in the presence of the both samples. Wear behavior of Ti6Al4V and the ODL samples was investigated in a phosphate buffered saline solution under a normal load of 30 N at a sliding velocity of 0.1 m/s. The worn surface and subsurface of the samples were studied using SEM, STEM, TEM, XPS, AFM, nano-hardness and surface profilometry. A bio-tribofilm was observed on the worn surface of the ODL. TEM studies showed that the tribofilm had an amorphous structure and contained oxygen and phosphorous as confirmed by XPS and EDS analysis. AFM images also revealed that the tribofilm consisted of compacted fine debris. The

formation of the tribofilm on the ODL with higher hardness and strength resulted in a decrease of about 95% in the wear rate compared with Ti6Al4V alloy.

**Keywords:** Ti6Al4V; Oxygen Diffusion Layer; Bio-tribofilm; TEM; XPS.

## 1. Introduction

Titanium and its alloys are widely used in various bio-applications [1,2]. Titanium alloys used in the human body are typically classified into three groups: a)  $\alpha$ -Ti, b)  $(\alpha+\beta)$ -Ti, and c)  $\beta$ -Ti [3,4]. The good performance of titanium alloys in the body is due to their excellent biocorrosion, non-toxicity and good osseointegration [5,6]. The passive oxide film formed on the surface of titanium alloys plays a major role in their prominent bio-properties; i.e., excellent corrosion resistance and biocompatibility [7]. However, low wear and tribocorrosion resistance of titanium is the drawback for artificial joint applications [8,9]. According to the literature, this is attributed to the low shear resistance of titanium and the lack of protection by a surface film [10]. The passive oxide film formed on the surface of titanium can be damaged by the mechanical loads during tribological processing. This may result in direct contact between the very reactive titanium and the corrosive medium, which causes a decrease in the properties, i.e., corrosion resistance and osseointegration [11,12]. In addition, the debris formed by wear may reduce the biocompatibility by release of toxic ions into the body [13]; leading to long-term health problems such as alzheimer, neuropathy and osteomalacia [14]. In some cases, the debris has also caused inflammation by the body immune system following first surgery [15]. The problem sometimes needs revision surgery, which has a lesser success probability than the first one according to the statistical data [5].

In joint applications, surface modifications have improved the wear resistance of titanium alloys by the formation of a bio-tribofilm [16,17]. The effect of tribofilm is highly related to its properties; i) its adhesion and surface chemical activity, ii) its shear resistance and lubricant properties and iii) the durability of tribofilm [18,19]. Among all surface engineering methods to be used to improve wear and tribocorrosion properties of titanium-based alloys for the bio-applications, thermal oxidation is easily applied and cost effective [20]. During thermal processing, titanium and oxygen react with each other and the surface will be covered by titanium oxide; i.e.  $\text{TiO}_2$ . Borgioli et al. [21] reported that the oxide layer formed on Ti6Al4V alloy consists of alternate layers of  $\text{TiO}_2$  and  $\text{Al}_2\text{O}_3$ . These two oxides have different physical properties; the resultant layer is almost porous and inhomogeneous and is not well-protective. Beside the oxidation reaction, oxygen atoms also diffuse into the titanium crystal structure and locate in the interstitial sites [22]. This is due to the combined effect of three parameters: inward diffusion of oxygen, high solubility of oxygen in titanium and smaller atomic radius of oxygen than titanium [10,23]. The result is the formation of an oxygen diffusion layer (ODL) just beneath the oxide layer on titanium alloys.

In this study, in vitro tests for cytotoxicity and tribocorrosion experiments were conducted on oxygen diffusion layer (ODL) and the results were compared with the untreated Ti6Al4V. In addition, a bio-tribofilm formed on the ODL sample was detected and characterized. The mechanism of formation of the bio-tribofilm on the treated sample was investigated.

## 2. Experimental Procedure

### 2.1. Samples preparation and thermal oxidation

Ti6Al4V bar with a diameter of 32 mm was obtained with the chemical composition listed in Table 1. The bar was sliced to disk-shape specimens with a thickness of 4 mm. The specimens were polished by a 600 grit SiC paper to reach an average surface roughness ( $R_a$ ) of about 0.14  $\mu\text{m}$ . The specimens were ultrasonically cleaned in acetone for six minutes. To produce oxygen diffusion layer (ODL) on the surface of the alloy, the specimens were placed in an air atmospheric furnace and heat treated at a temperature of 850 °C for six hours. The relative humidity of the atmosphere was measured to be 40%. The thermal oxidation led to the formation of an oxygen diffused layer with a thin weak oxide layer on the top. The heat-treated specimens were then quenched at room temperature to detach the loosely oxide layer. The treated samples were lightly polished to remove the remained oxide scales from the surfaces. The samples were again ultrasonically cleaned in the acetone solution. The nano-hardness measurements of the surface and subsurface of the treated, i.e., the ODL and untreated (Ti6Al4V) samples were obtained under an applied load of 10 mN with a loading/unloading rate of 0.2 mN/s.

**Table 1** Chemical composition of Ti-6Al-4V alloy (wt%)

	Ti	Al	V	Fe	Mo	Si	Cu	W	Nb	Ni	Sn	Mn
Base	6.37	4.33	0.03	0.01	0.01	0.01	<0.01	0.008	<0.005	<0.005	<0.005	<0.004

## 2.2. Cytotoxicity assay

In vitro tests for cytotoxicity were carried out by a direct contact method in accordance with BS EN ISO 10993-5 [24]. Disks with a diameter of 7 mm were prepared from Ti6Al4V and the

ODL samples. The samples were then sterilized in an autoclave at a temperature of 120 °C for 30 minutes. In vitro cell tests were conducted on the samples by using osteoblast-like G292 Cells in the RPMI-1640 medium with 10% fetal calf serum.

The cells with a density of  $1\times10^4$  cells/ml were seeded directly onto the Ti6A14V and ODL specimens. The cell culture was carried out in an incubator at a temperature of  $37\pm0.5$  °C in a 5% CO<sub>2</sub> humidified atmosphere. The cells incubated in the culture medium with no specimen were considered as the controls. After 24 hours of cell culturing, the cell viability was evaluated by adding 3-(4,5-dimethylthiazol-2yl)-2,5-diphenyl-tetrazolium bromide (MTT) assay to the cell medium. A culture medium containing MTT was placed into each well of a 96-well plate, and the cells were cultured for 4 hours in the incubator at a temperature of 37 °C in a 5% CO<sub>2</sub> humidified atmosphere. The viable cells could easily metabolize the tetrazolium salt by the formation of purple formazan crystals. The formed formazan crystals were then solubilized by adding dimethyl sulfoxide (DMSO). After the solubilization of the purple formazan crystals, the optical density of the solution, which indicated the number of viable cells, was measured by using an enzyme-linked immunoadsorbent assay (ELISA) reader at a wavelength of 570 nm. The data were then compared with the results of the controls, which were considered as 100% cell viability.

### 2.3. Tribocorrosion tests

The tribocorrosion experiments were conducted on the treated and untreated samples using a unidirectional ball-on-disk tribometer [26] in a phosphate buffered saline (PBS) solution under a normal load of 30 N and at sliding speed of 0.1 m/s (160 RPM) for a sliding distance of 1000 m. The PBS was prepared in accordance with ASTM F2129 [25], which consisted of 8.0 g/l NaCl,

1.15 g/l Na<sub>2</sub>HPO<sub>4</sub>, 0.2 g/l KCl and 0.2 g/l KH<sub>2</sub>PO<sub>4</sub> in distilled water. The PBS container and the specimen holder were made of a polymeric material and mounted on the tribometer. Alumina balls, 5 mm in diameter with a hardness of 18.3 GPa (1870 Hv), were selected as the counterparts. All tests were repeated for at least three times and the mean values and standard deviations were reported.

Before and after the tribocorrosion tests, the specimens were weighed by a balance with an accuracy of 10<sup>-4</sup> g. The profiles of the wear tracks were obtained using a T-8000 HommelWerke surface stylus profilometer. The change in the nano-hardness of the material beneath the wear tracks were also measured. The wear surfaces were studied by a Bruker Atomic Force Microscope (AFM) using peak force tapping technique with a peak force set-point of 1.5  $\mu$ N and a frequency of 2 kHz.

#### 2.4. Microscopy and material characterization

The wear surfaces were further studied by a FEI Scanning Electron Microscope (SEM) equipped with an Energy Dispersive Spectroscopy (EDS). The chemical composition of the tribocorrosion surfaces was further investigated by the spectra of X-ray Photoelectron Spectroscopy (XPS). The variation in the chemical composition along the depth under the wear tracks were characterized by XPS with the measurement steps of about 60-65 nm from the wear surface. In addition, the microstructure of the subsurface of wear tracks was analyzed using Transmission Electron Microscope (TEM). To prepare TEM specimens, the Focus Ion Beam (FIB) lift-out technique was used and a membrane of the surface material was obtained using a gallium ion beam in the SEM chamber. Before the bombardment by gallium ion, the area of the wear surface was coated with platinum to avoid the microstructural changes during ion milling. A

membrane was obtained from the wear surface of Ti6Al4V and the ODL samples for TEM studies. The membranes were then fixed in the TEM grids by CVD deposition of platinum. TEM specimens with a thickness of less than 100 nm were then prepared by a sequential ion milling. TEM dark-field and bright-field images, Selected Area Electron Diffraction (SAED) patterns and EDS elemental maps were obtained using a FEI Titan Themis TEM operated at 300 kV equipped with a High Angle Annular Dark Field (HAADF) detector for Scanning Transmission Electron Microscope (STEM) imaging.

### 3. Results

#### 3.1. Cytotoxicity

The cell viability in the presence of Ti-6Al4V and the ODL were assessed after 24 hours of the cell culture and the results are shown in Fig. 1. The figure shows a lower cell viability property of the ODL compared with Ti6Al4V. However, there was no statistically significant difference ( $p<0.05$ ) between the data for the both samples and the controls, indicating an appropriate cytocompatibility of the samples. The similar cell viability in the presence of the samples revealed that there was no meaningful effect of the oxygen diffusion treatment on the cytotoxicity of the alloy.

It is believed that, although, the release of aluminum and vanadium ions from Ti6Al4V could be cytotoxic [13]; the formation of a passive film could cover the alloy surface and avoid the significant release of the detrimental ions in human body. This is the main reason that Ti6Al4V alloy is still used as the load bearing implants [27].

#### 3.2. Nano-hardness

The nano-indentation tests were performed on the surfaces of the treated (ODL) and untreated (Ti6Al4V) samples. The variation of indentation load as a function of penetration depth for both samples is illustrated in Fig. 2. During unloading, some deformation (i.e., penetration depth) was recovered indicating the amount of elastic deformation of each material. The remaining indentation depth was permanent and considered as the plastic deformation. Table 2 shows the data that were obtained from the nano-indentation tests in Fig. 2. A lower value of plastic displacement of the ODL (90 nm) compared with 220 nm for Ti6Al4V could indicate a higher hardness of the ODL. Nano-hardness measurement for the ODL and Ti6Al4V samples in the table revealed the value of about 19.1 GPa (1950 Hv) and 5.0 GPa (500 Hv), respectively. The higher hardness of the ODL sample was attributed to the presence of oxygen in interstitial sites of titanium structure due to oxygen diffusion during the thermal oxidation treatment. It is believed that the interstitial oxygen increased the stress fields within the structure and limited the amount of plastic flow [28] that resulted in an increase in the hardness. The elastic moduli could be obtained from the elastic penetration depths [29] in Fig. 2. The values of about 246 GPa and 164 GPa were obtained for the ODL and Ti6Al4V samples, respectively, as listed in Table 2. E/H values were then calculated as presented in Table 2. A decrease of about 60% in E/H ratio was observed after the thermal treatment (i.e., on the ODL sample) due to the oxygen diffusion. A lower E/H ratio could result in a more brittle behaviour of the ODL wear surface [30] as would be discussed later.

**Table 2** Mechanical parameters from the nano-indentation data in Fig. 2

Sample	H, GPa	E, GPa	E/H Ratio	Elastic Depth, nm	Plastic Depth, nm
Ti6Al4V	5.0±0.5	164±7.1	32.8±1.8	69±3	223±19
ODL	19.1±1.1	246±5.8	12.9±0.3	73±7	90±11

The change in the nano-hardness of the ODL sample with distance from the surface before a wear test is illustrated in Fig. 3a. The hardness was increased from a value of about 600 Hv in the substrate to about 1950 Hv on the surface of the sample. This revealed the effect of oxygen concentration on the hardness of Ti6Al4V alloy, i.e., the higher oxygen concentration on the surface resulted in a higher hardness. The nano-hardness of the subsurface of both samples after the wear tests was also measured and the results are shown in Fig. 3b. There was a sharp decrease in the hardness of Ti6Al4V from 900 Hv close to the wear surface to a value of about 500 Hv (i.e., the hardness of untreated Ti6Al4V) at about 10  $\mu\text{m}$  below the wear surface.

### 3.3. Wear Rate

The wear rates of the samples and their alumina counterparts are presented in Fig. 4. The figure shows that although the wear rates of the alumina balls mating with the samples were about the same, the thermal oxidation treatment of Ti6Al4V alloy decreased the wear rate of the alloy by about 95%. However, a similar cytocompatibility of the ODL and Ti6Al4V was observed as shown in Fig. 1. This could nominate the ODL as an alternative for Ti6Al4V alloy in joint applications where the weak wear resistance of Ti6Al4V could cause health problems.

The higher surface hardness of the ODL sample could be a reason for its lower wear rate. However, Fig. 3b shows that the subsurface hardness of Ti6Al4V increased to a value close to that of the ODL sample due to work hardening during wear. This suggested that other parameters than hardness could also affect the wear behaviour of the samples. The subject was investigated using various techniques including SEM, TEM, XPS and AFM and will be discussed in the following sections.

### 3.4. Surface and Subsurface Examinations

Figure 5 shows SEM micrographs of the wear tracks of Ti6Al4V and the ODL samples under a normal load of 30 N. A much roughened surface with plastically deformed features along with abrasive grooves could be observed on the worn surface of untreated Ti6Al4V sample in Fig. 5a. For the ODL sample, however, a smoother wear surface with no abrasive grooves could be seen in Fig. 5b as compared with the untreated sample. The absence of abrasive grooves on the wear surface of the ODL sample was attributed to a lower E/H value and a limited plastic deformation of the oxygen diffusion layer in Fig. 2. The lower hardness and strength of Ti6Al4V under a normal load of 30 N could enable the material to deform easily during wear, resulting in the well-defined grooves in Fig. 5a. This was in agreement with the higher E/H ratio obtained in Ti6Al4V sample, indicating higher ability to plastic deformation [30].

There were some darker regions indicative of tribofilm formation on the wear surface of the ODL in Fig. 5b and was investigated by EDS elemental maps and XPS analysis. Figure 6 shows HAADF STEM image of the cross section of the wear track of the ODL sample. The corresponding EDS elemental maps are also shown in the figure. The tribofilm on the wear surface of the treated sample (i.e., the ODL) could be obviously seen in the figure. The EDS map analysis revealed that the layer was a mixture containing the elements of Ti6Al4V alloy and oxygen and some phosphorous and sodium from the saline solution. It is interpreted that the formation of tribofilm resulted from the tribo-reaction of the ODL surface with the simulated body fluid containing phosphorous and sodium ions.

Due to high surface sensitivity (i.e., top few atomic layers) of XPS analysis, the analyses could be indicative of the analysis of the tribofilm formed during tribocorrosion. The change in the

oxygen and phosphorous concentrations with distance from the wear surface of both samples obtained from the survey spectra of the XPS analysis is presented in Fig. 7. The XPS analysis of Fig. 7a shows an oxygen content of about 40 at% to the depth of at least 560 nm on the wear surface of the ODL. However, our data on the EDS analysis of the unworn ODL showed a maximum content of 20 at% oxygen on the surface. This could suggest the formation of a tribofilm with a higher oxygen content on the wear surface of the ODL. High-resolution XPS spectra of O 1s, P 2p and Ti 2p were obtained from the wear surface of the ODL and are shown in Fig. 8. The O 1s spectrum was fitted with five peaks at various binding energies, indicating the presence of oxygen in different states. According to the literature [31], the peaks at the binding energies of 530.6 and 531.8 eV were attributed to oxygen in  $\text{TiO}_2$  and  $\text{Al}_2\text{O}_3$ , respectively. In Fig. 8a, the peaks at the binding energy of 531.2 eV could be due to a phosphate compound [32], and other peaks at 532.5 and 533.4 eV corresponded to the adsorbed oxygen [31] on the surface.

Figure 7 shows a high amount of oxygen (i.e., 40 at%) and phosphorous (i.e., 3 at%) at the near surface of Ti6Al4V, which decreased sharply in the regions deeper than 100 nm. The existence of phosphorous and oxygen on the worn surface of Ti6Al4V sample might be related to the formation of a very thin (i.e., about 100 nm) tribofilm during tribocorrosion. Figure 7b also shows a higher content of phosphorous in the deeper subsurface regions of the treated (i.e., the ODL) sample, i.e., at least 560 nm from the worn surface. It should be mentioned that the only source of phosphorous was from the solution, and phosphorous could not diffuse in the metal lattice at room temperature. Therefore, the presence of phosphorous on the surface and subsurface of the ODL wear sample could confirm the existence of tribofilm with a thickness of at least 560 nm. In addition, as shown in Fig. 8b, the high-resolution P 2p spectrum was fitted

with three peaks at various binding energies. The peaks at the binding energies of 133.0, 133.8 and 134.8 eV corresponded to phosphorous in  $\text{PO}_4^{3-}$ ,  $\text{HPO}_4^{2-}$  and  $\text{H}_2\text{PO}_4^-$  components, respectively [32,33].

The presence of phosphates was also confirmed in Fig. 8c, where the peaks of the Ti 2p spectrum at 460.0 and 466.4 eV were attributed to titanium phosphate [34]. The Ti 2p spectrum also indicated the presence of  $\text{TiO}_2$  by the peaks at the binding energies of 459.3 and 465.3 eV, which were corresponded to  $\text{Ti } 2\text{p}_{3/2}$  and  $\text{Ti } 2\text{p}_{1/2}$ , respectively. The spectrum in Fig. 8c presents two other peaks at 458.6 and 464.0 eV, which might result from a titanium oxide with a lower valence of titanium (i.e.,  $\text{TiO}_x$ ) [33]. Therefore, the XPS analyses confirmed that the tribofilm contained a mixture of titanium oxides and phosphates.

Figure 9 shows TEM images of the wear cross section of Ti6Al4V. The Selected Area Electron Diffraction (SAED) patterns obtained from various locations below the wear surface are also illustrated in Fig. 9. There was a platinum coating on the surface, which protected the surface from gallium ion bombardments during FIB processing. A continuous thin layer of about 20 nm on the wear surface was also due to the platinum coating. At the regions beneath the platinum coating, the nano-crystalline grains with the size of less than 50 nm could be observed in Fig. 9b. The formation of very fine grains was due to high strain and strain rates exerted on the underlying material during sliding that also caused an increase in the nano-hardness of Ti6Al4V as shown in Fig. 3b. The continuous ring of the SAED pattern in Fig. 9d from region 1 of Fig. 9b also suggested the formation of nano-crystalline structure. The diffraction pattern also shows two continuous rings from (100) and (101) planes of  $\alpha$ -Ti and very few diffractions from the higher indices planes. However, the diffraction patterns from deeper regions (point 2 in Fig. 9b and point 3 in Fig. 9c) show less continuous rings diffracted from (100) and (101) planes

but with more diffraction from other planes. The patterns suggest that there were higher strain and strain rates closer to the wear surface which could result in a preferential orientation of the  $\alpha$ -Ti grains to (100) and (101) planes near the wear surface.

Grains of  $\alpha$ -Ti with a size less than 200 nm could be observed in the deeper regions, i.e., point 3 in Fig. 9c, about 5000 nm from the wear surface of Ti6Al4V. The low index rings in the SAED pattern were also changed from a continuous ring pattern near the wear surface in Fig. 9d (i.e., point 1 in Fig. 9b) to discrete spots in the deeper regions in Fig. 9f, which confirmed the electron diffraction from coarser grains.

The dark-field TEM image and SAED patterns at the various locations of the subsurface regions of the wear surface of the ODL sample are presented in Fig. 10. Below the platinum coating, Fig. 10 shows that a discontinuous tribofilm with a varying thickness less than 230 nm was formed. There were no cracks or defects at the interface between the tribofilm and the ODL substrate, which could suggest a good adhesion. Figure 10a shows larger grains at the deeper regions (i.e., 4 or 5  $\mu\text{m}$ ) as compared with the grains close to the wear surface. The diffraction pattern obtained at region 2 about 100 nm away from the wear surface in Fig. 10c indicated relatively more continuous rings than the regions further away from the wear surface. In the deeper locations about 500-2000 nm from the wear surface, the diffraction patterns were changed to spot patterns (Figs. 10d-g). The SAED patterns revealed that the grain refinement in the ODL sample was limited to a thin layer with a thickness of about 500 nm, which was much lower than the depth (i.e., at least 5000 nm) of the grain-refined region in the untreated sample in Fig. 9.

Figure 10b shows a diffraction pattern obtained from the tribofilm. The diffraction pattern confirms that an amorphous structure was obtained in the tribofilm. The high strains and strain rates very close to the sliding surface resulted in a mechanically mixed layer [30] consisting of

wear debris, chemical compounds formed with the solution and mixed with the deformed material on the ODL surface producing an amorphous tribofilm. Figures 6 and 8 confirmed the formation of the layer consisting of various elements and compounds, respectively.

In order to verify that the tribofilm contained compacted fine particles, AFM studies were conducted on the wear surface of the ODL. Figure 11 illustrated the AFM image of the wear track of the ODL sample. There was a scratch with a depth of about 2.5  $\mu\text{m}$  in the upper right corner of the 3D image. AFM 2D high sensor images of the rectangular areas in Fig 11a are presented in Figs. 11b and c. Figure 11b shows a region on the surface where a very thin (about 70 nm) film or narrow wear grooves was formed. However, Fig. 11c shows a thicker film in a part of region 2 with a thickness of around 400 nm. The figure shows that the tribofilm consisted of fine particles of about 250 nm in diameter.

## 4. Discussion

### 4.1. Plastic Deformation of the Subsurface of Wear Tracks

The change in nano-hardness with distance from the wear surface in Fig. 3b indicated an increase of about 80% in the hardness of Ti6Al4V due to the induced stresses on the near surface regions during sliding wear and subsequent plastic deformation and work hardening of the material. The decrease in the hardness with distance from the wear surface was also observed for the ODL sample; however, it was not as sharp as Ti6Al4V. The result suggested that the subsurface plastic deformation on the ODL did not show work hardening and a tangible effect on the hardness of wear subsurface region as was depicted for Ti6Al4V.

The microstructural studies of Ti6Al4V before wear test showed that the bulk material contained  $\alpha$ -Ti grains with an average size of about 4000 nm and remained  $\beta$ -Ti in the grain boundaries.

The formation of very fine grains of Ti6Al4V in the TEM image of Fig. 9 was due to high strain and strain rates exerted on the underlying material during sliding that also caused an increase in the nano hardness of Ti6Al4V as shown in Fig. 3b. The smaller grain size in region 3 in Fig. 9c compared with the grain size of the bulk material revealed that the material 5000 nm away from the wear surface was also affected by deformation and work hardening during sliding. The formation of the fine grains at the subsurface of Ti6Al4V during wear also resulted in an increase in the hardness of these regions as presented in Fig. 3b. It should be mentioned that due to the limitation of the FIB sampling it was not possible to study the microstructure of the sample by TEM at deeper regions, i.e., more than 5000 nm (5  $\mu\text{m}$ ). However, the hardness measurements shown in Fig. 3b indicated that the increase in hardness and, therefore, plastic deformation occurred at a depth of about 10  $\mu\text{m}$  from the wear surface of Ti6Al4V under a normal load of 30 N in a PBS solution. The plastic deformation of the surface and subsurface could limit the formation of tribofilm on the wear surface [35] and, therefore, limit the protection needed to reduce wear of Ti6Al4V in Fig. 4.

The mechanisms of the grain refinement of Ti6Al4V during sliding wear could be explained as follow: Ti6Al4V alloy has high stacking fault energy with a dual phase ( $\alpha + \beta$ ) structure;  $\alpha$  and  $\beta$  phases have hexagonal close-packed (hcp) and body centered cubic (bcc) crystal structures, respectively [36]. Titanium with hcp structure has higher number of packed planes than other hcp metallic materials [37]. This is related to its c/a ratio of 1.587, which is lower than the value of 1.633 for ideal hcp structure. The lower c/a ratio results in more densely packed prismatic and pyramidal planes, i.e.,  $\{10\bar{1}0\}$  and  $\{10\bar{1}1\}$ . This causes slip to also occur in these planes as in the basal planes  $\{0001\}$  and, therefore, to increase the slip systems [38]. However, the number of slip systems of  $\alpha$ -Ti are not high enough for the plastic flow by the dislocation slip mode [39].

In fact, only four independent slip systems are provided by the basal, prismatic and pyramidal slip planes [39], whereas, at least five independent slip systems are required for compatible plastic deformation in accordance with Von-Mises criterion [40].

It is believed that the formation of deformation twins is the dominant mechanism to accommodate plastic deformation of  $\alpha$ -Ti with a coarse grained microstructure [41] as occurred during early stage of deformation of alpha grains of Ti6Al4V. However, no deformation twins were observed in the TEM images of the nanostructure of Ti6Al4V wear contact region in Fig. 9. Kim et al. [42] reported a similar observation on deformation of pure  $\alpha$ -Ti microstructure alloy (i.e., CP-Ti) after its grains were refined to nano-scale by ECAP. It has been proposed [43] that in a metallic material with a nano-grained structure, even those with limited slip systems such as  $\alpha$ -Ti, compatible plastic deformation might be accommodated by slip without the formation of twinning. Therefore, the requirement of five independent slip systems was not needed to accommodate deformation by dislocation slip for highly refined grains [44]. Furthermore, it was also suggested [44] that several nano-grains should simultaneously deform plastically to meet the Von-Mises criterion in order to have deformation by dislocation slip mode. On the other hand, the remaining beta phase ( $\beta$ -Ti) with bcc structure and more independent slip systems and high stacking fault energy could easily deform by dislocation slip mode [36].

During wear, the simultaneous effects of these two deformation mechanisms (i.e., deformation twin and dislocation slip modes) could generate dislocation walls by intersections between twins and dislocations [36]. The dislocation walls divide the grain into several sub-grains and result in submicron and nano-scaled grains [45] as shown in Fig. 9b.

The surface profilometry of the wear track of the ODL sample under a normal load of 30 N showed that the depth of wear track was about 30  $\mu\text{m}$ . Figure 3a indicates that the hardness of

the unworn ODL at a distance of 30  $\mu\text{m}$  from the surface was about 800 Hv. This value was very close to the measured hardness of the near surface region of the wear track of the ODL in Fig. 3b. This revealed that the hardness of the regions near the wear surface in the ODL sample was directly related to the amount of diffused oxygen and not the plastic deformation induced by wear.

The much lower depth of the grain refinement region in the ODL sample (Fig. 10) also indicated a low depth of plastic deformation induced by the contact stresses during sliding. This could be due to the diffusion of oxygen atoms in the interstitial positions of  $\alpha$ -Ti which increased the hardness and c/a ratio of the hcp structure [23]. The higher c/a ratio limited the slip systems [10] and the higher hardness lowered the depth of plastic deformation during sliding. Comparing the subsurface hardness of the ODL wear surface in Fig. 3b and the SAED patterns in Fig. 10 suggested that, although there was a slight change in the diffraction patterns at 250 and 500 nm depth, but there was not any meaningful change in the variation of the hardness during sliding. This confirmed that the diffusion process rather than the mechanical factors, i.e., the plastic deformation and work hardening, controlled the hardness of the subsurface regions in the ODL sample.

#### **4.2. Bio-Tribofilm Formation on the ODL**

The tribofilm was observed on the wear surface of the ODL sample as shown in SEM images of the wear tracks in Fig. 5. The formation of the film was also confirmed by the STEM and TEM cross-sectional studies shown in Figs. 6 and 10, respectively. The High-resolution XPS spectra in Fig. 8 showed that the bio-tribofilm contained  $\text{Al}_2\text{O}_3$ ,  $\text{TiO}_2$ , titanium phosphates and adsorbed

oxygen. These results revealed the reaction of the ODL surface with the PBS solution to form a bio-tribofilm on the wear surface.

Interstitial oxygen in titanium structure might control the tribofilm formation and its durability by the combination of two following factors: (1) The probability of wear particle formation during sliding increased with a decrease in E/H ratio, due to a more brittle behaviour of the material during sliding [30]. Therefore, due to a lower E/H of the ODL (Fig. 2), a higher fraction of the wear track could become wear debris as compared with Ti6Al4V. The debris were then compacted during sliding leading to the formation of tribofilm on the wear surface. The SAED pattern of Fig. 10b and the XPS data of Fig. 8 and the AFM image of Fig. 11c suggest that the tribofilm was amorphous and consisted of fine particles of compounds of titanium and aluminum oxides and titanium phosphates. (2) On the other hand, the tribofilm was formed on the surface of the ODL with a higher hardness, which did not change with depth and the subsurface deformation. This made the ODL subsurface more stable to support the tribofilm and hinder its break-down under a normal load of 30 N as observed in Figs. 5b, 6 and 10a. The existence of a durable tribofilm on the wear surface limited the mating contact and was a reason for the lower wear rate of the ODL sample compared with Ti6Al4V in Fig. 4. The SAED pattern of Ti6Al4V subsurface (Figs. 9d-f) with a lower hardness revealed that the deformation existed in the depth much greater than the ODL sample. This high deformation made the substrate unstable for tribofilm to form on Ti6Al4V during sliding.

## 5. Conclusions

- 1- The diffusion of oxygen in Ti6Al4V during thermal oxidation processing resulted in an ODL surface with a higher hardness and a lower E/H ratio.

- 2- In vitro tests for cytotoxicity indicated a similar cytocompatibility for Ti6Al4V and the ODL samples.
- 3- A decrease of about 95% in the wear rate of the ODL was observed as a result of thermal processing. This was attributed to the higher hardness of the ODL sample as well as formation of an amorphous tribofilm on the worn surface as detected in SEM, TEM and AFM images.
- 4- XPS analysis showed that the tribofilm contained aluminum and titanium oxides and titanium phosphates.
- 5- TEM results indicated that the grain refinement in the ODL occurred close to the wear surface at a depth of about 500 nm, while the affected depth for Ti6Al4V sample was at least 5  $\mu$ m. The much lower depth of grain refinement in the ODL sample was related to the oxygen diffusion and its lower ability for plastic deformation, which resulted in a better support for the bio-tribofilm.
- 6- The AFM study showed that the tribofilm was consisted of fine particles.

## References

- [1] J.E.G. González, J.C. Mirza-Rosca, Study of the corrosion behavior of titanium and some of its alloys for biomedical and dental implant applications, *J. Electroanal. Chem.* 471 (1999) 109–115. doi:10.1016/S0022-0728(99)00260-0.
- [2] Q. Chen, G.A. Thouas, Metallic implant biomaterials, *Mater. Sci. Eng. R Reports.* 87 (2015) 1–57. doi:10.1016/j.mser.2014.10.001.
- [3] M. Geetha, a. K. Singh, R. Asokamani, a. K. Gogia, Ti based biomaterials, the ultimate choice for orthopaedic implants - A review, *Prog. Mater. Sci.* 54 (2009) 397–425.

doi:10.1016/j.pmatsci.2008.06.004.

- [4] M. Niinomi, Recent titanium R&D for biomedical applications in japan, *Jom.* 51 (1999) 32–34. doi:10.1007/s11837-999-0091-x.
- [5] M. Long, H.J. Rack, Titanium alloys in total joint replacement—a materials science perspective., *Biomaterials.* 19 (1998) 1621–1639. doi:10.1016/S0142-9612(97)00146-4.
- [6] R. Adell, U. Lekholm, B. Rockler, P.I. Bränemark, A 15-year study of osseointegrated implants in the treatment of the edentulous jaw., *Int. J. Oral Surg.* 10 (1981) 387–416. doi:10.1016/S0300-9785(81)80077-4.
- [7] J. Pan, D. Thierry, C. Leygraf, Electrochemical impedance spectroscopy study of the passive oxide film on titanium for implant application, *Electrochim. Acta.* 41 (1996) 1143–1153. doi:10.1016/0013-4686(95)00465-3.
- [8] R. Yazdi, S.F. Kashani-Bozorg, Microstructure and wear of in-situ Ti/(TiN + TiB) hybrid composite layers produced using liquid phase process, *Mater. Chem. Phys.* 152 (2015). doi:10.1016/j.matchemphys.2014.12.026.
- [9] B.A. Obadele, A. Andrews, P.A. Olubambi, M.T. Mathew, S. Pityana, Tribocorrosion behaviour of laser cladded biomedical grade titanium alloy, *Mater. Corros.* 66 (2015) 1133–1139. doi:10.1002/maco.201408037.
- [10] F.H. Froes, ed., Principles of Alloying Titanium, in: *Titan. Phys. Metall. Process. Appl.*, 1st Editio, ASM International, Ohio, 2015: pp. 51–74.
- [11] V. Totolin, V. Pejaković, T. Csanyi, O. Hekele, M. Huber, M. Rodríguez Ripoll, Surface engineering of Ti6Al4V surfaces for enhanced tribocorrosion performance in artificial

seawater, Mater. Des. 104 (2016) 10–18. doi:10.1016/j.matdes.2016.04.080.

- [12] H. Haleem-Smith, E. Argintar, C. Bush, D. Hampton, W.F. Postma, F.H. Chen, et al., Biological responses of human mesenchymal stem cells to titanium wear debris particles, J. Orthop. Res. 30 (2012) 853–863. doi:10.1002/jor.22002.
- [13] R.M. Pilliar, Metallic biomaterials, Biomed. Mater. (2009) 41–81. doi:10.1007/978-0-387-84872-3\_2.
- [14] G. Manivasagam, D. Dhinasekaran, A. Rajamanickam, Biomedical Implants: Corrosion and its Prevention - A Review, (2010). doi:10.2174/1877610801002010040.
- [15] L. Burton, D. Paget, N.B. Binder, K. Bohnert, B.J. Nestor, T.P. Sculco, et al., Orthopedic wear debris mediated inflammatory osteolysis is mediated in part by NALP3 inflammasome activation, J. Orthop. Res. 31 (2013) 73–80. doi:10.1002/jor.22190.
- [16] D. Choudhury, J.M. Lackner, L. Major, T. Morita, Y. Sawae, A. Bin Mamat, et al., Improved wear resistance of functional diamond like carbon coated Ti–6Al–4V alloys in an edge loading conditions, J. Mech. Behav. Biomed. Mater. 59 (2016) 586–595. doi:10.1016/j.jmbbm.2016.04.004.
- [17] A. Bandyopadhyay, S. Dittrick, T. Gualtieri, J. Wu, S. Bose, Calcium phosphate-titanium composites for articulating surfaces of load-bearing implants, J. Mech. Behav. Biomed. Mater. 57 (2016) 280–288. doi:10.1016/j.jmbbm.2015.11.022.
- [18] C. Rynio, H. Hattendorf, J. Klöwer, G. Eggeler, The evolution of tribolayers during high temperature sliding wear, Wear. 315 (2014) 1–10. doi:10.1016/j.wear.2014.03.007.
- [19] Y.S. Mao, L. Wang, K.M. Chen, S.Q. Wang, X.H. Cui, Tribo-layer and its role in dry

sliding wear of Ti-6Al-4V alloy, Wear. 297 (2013) 1032–1039.

doi:10.1016/j.wear.2012.11.063.

- [20] Y. Luo, W. Chen, M. Tian, S. Teng, Thermal oxidation of Ti6Al4V alloy and its biotribological properties under serum lubrication, Tribol. Int. 89 (2015) 67–71.  
doi:10.1016/j.triboint.2014.12.022.
- [21] F. Borgioli, E. Galvanetto, A. Fossati, G. Pradelli, Glow-discharge and furnace treatments of Ti-6Al-4V, Surf. Coatings Technol. 184 (2004) 255–262.  
doi:10.1016/j.surfcoat.2003.10.004.
- [22] H. Dong, X.Y. Li, Oxygen boost diffusion for the deep-case hardening of titanium alloys, Mater. Sci. Eng. A. 280 (2000) 303–310. doi:10.1016/S0921-5093(99)00697-8.
- [23] S. Zabler, Interstitial Oxygen diffusion hardening - A practical route for the surface protection of titanium, Mater. Charact. 62 (2011) 1205–1213.  
doi:10.1016/j.matchar.2011.10.012.
- [24] BS EN ISO 10993-5, Biological evaluation of medical devices-Part 5: Tests for in vitro cytotoxicity, Switzerland, 2009.
- [25] ASTM F2129-15, Standard Test Method for Conducting Cyclic Potentiodynamic Polarization Measurements to Determine the Corrosion Susceptibility of Small Implant, 2015.
- [26] R. Yazdi, H.M. Ghasemi, C. Wang, A. Neville, Bio-corrosion behaviour of oxygen diffusion layer on Ti-6Al-4V during tribocorrosion, Corros. Sci. (2017).  
doi:10.1016/j.corsci.2017.08.031.

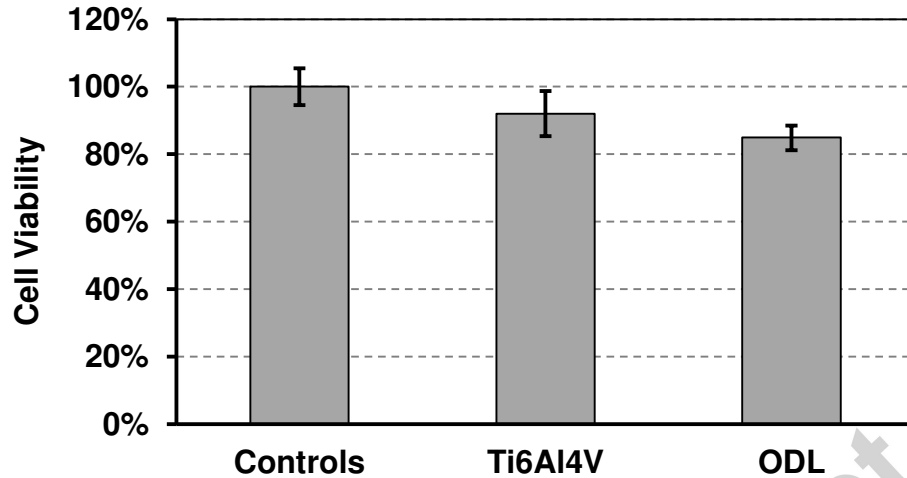
- [27] B. Sivakumar, S. Kumar, T.S.N. Sankara Narayanan, Fretting corrosion behaviour of Ti-6Al-4V alloy in artificial saliva containing varying concentrations of fluoride ions, *Wear.* 270 (2011) 317–324. doi:10.1016/j.wear.2010.09.008.
- [28] L.P. Lefebvre, E. Baril, M.N. Bureau, Effect of the oxygen content in solution on the static and cyclic deformation of titanium foams, *J. Mater. Sci. Mater. Med.* 20 (2009) 2223–2233. doi:10.1007/s10856-009-3798-x.
- [29] A.C. Fischer-Cripps, *Nanoindentation*, Third Edit, Springer Science & Business Media, London, 2011. doi:10.1007/978-1-4419-9872-9.
- [30] I. Hutchings, *Tribology-Friction and Wear of Engineering Materials*, First Edit, Butterworth-Heinemann, London, 1992.
- [31] Y. Luo, W. Chen, M. Tian, S. Teng, Thermal oxidation of Ti6Al4V alloy and its biotribological properties under serum lubrication, *Tribol. Int.* 89 (2015) 67–71. doi:10.1016/j.triboint.2014.12.022.
- [32] J.F. Moulder, W.F. Stickle, P.E. Sobol, K.D. Bomben, *Handbook of X-ray Photoelectron Spectroscopy*, Perkin-Elmer Corporation, Minnesota, 1992. doi:10.1002/sia.740030412.
- [33] T. Hanawa, M. Ota, Characterization of surface film formed on titanium in electrolyte using XPS, *Appl. Surf. Sci.* 55 (1992) 269–276. doi:10.1016/0169-4332(92)90178-Z.
- [34] M.F. Sunding, I.T. Jensen, P.M. Stenstad, S. Diplas, ARXPS and high energy XPS characterisation of titanium surfaces for medical implants, *Surf. Interface Anal.* 40 (2008) 751–753. doi:10.1002/sia.2778.
- [35] R. Aliasgarian, H.M. Ghasemi, M. Abedini, Tribological Behavior of Heat Treated Ni-rich

NiTi Alloys, J. Tribol. 133 (2011) 31602. doi:10.1115/1.4004102.

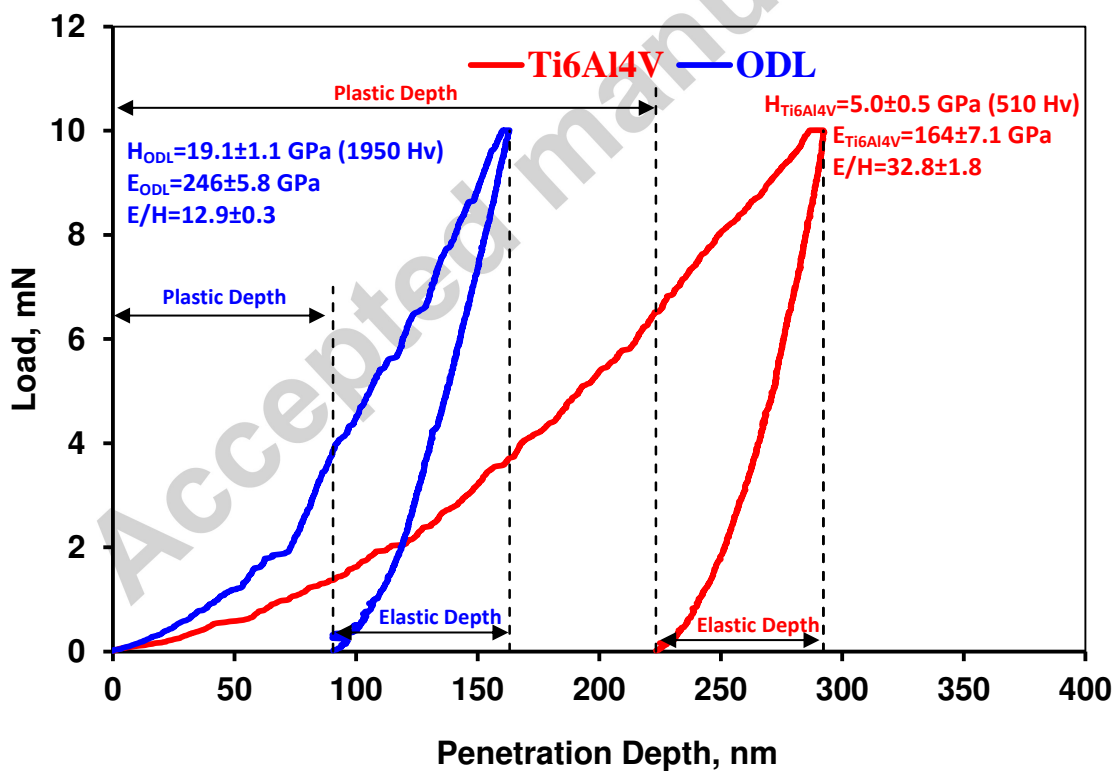
- [36] Y. Liu, M. Li, Nanocrystallization mechanism of beta phase in Ti-6Al-4V subjected to severe plastic deformation, Mater. Sci. Eng. A. 669 (2016) 7–13. doi:10.1016/j.msea.2016.05.088.
- [37] P.G. Partridge, The crystallography and deformation modes of hexagonal close-packed metals, Rev. Lit. Arts Am. 12 (1967) 169–194. doi:10.1179/mlta.1967.12.1.169.
- [38] C. Leyens, M. Peters, eds., Structure and Properties of Titanium and Titanium Alloys, in: Titan. Titan. Alloy. Fundam. Appl., John Wiley & Sons, 2006: pp. 1–36. doi:10.1002/3527602119.
- [39] A.A. Salem, S.R. Kalidindi, R.D. Doherty, Strain hardening of titanium: Role of deformation twinning, Acta Mater. 51 (2003) 4225–4237. doi:10.1016/S1359-6454(03)00239-8.
- [40] U.F. Kocks, Independent slip systems in crystals, Philos. Mag. 10 (1964) 187–193. doi:10.1080/14786436408225657.
- [41] A.A. Salem, S.R. Kalidindi, R.D. Doherty, S.L. Semiatin, Strain hardening due to deformation twinning in alpha-titanium: Mechanisms, Metall. Mater. Trans. A. 37 (2006) 259–268. doi:10.1007/s11661-006-0171-2.
- [42] I. Kim, J. Kim, D.H. Shin, X.Z. Liao, Y.T. Zhu, Deformation twins in pure titanium processed by equal channel angular pressing, Scr. Mater. 48 (2003) 813–817. doi:10.1016/S1359-6462(02)00513-4.
- [43] M.R. Shankar, B.C. Rao, S. Lee, S. Chandrasekar, A.H. King, W.D. Compton, Severe

plastic deformation (SPD) of titanium at near-ambient temperature, *Acta Mater.* 54 (2006) 3691–3700. doi:10.1016/j.actamat.2006.03.056.

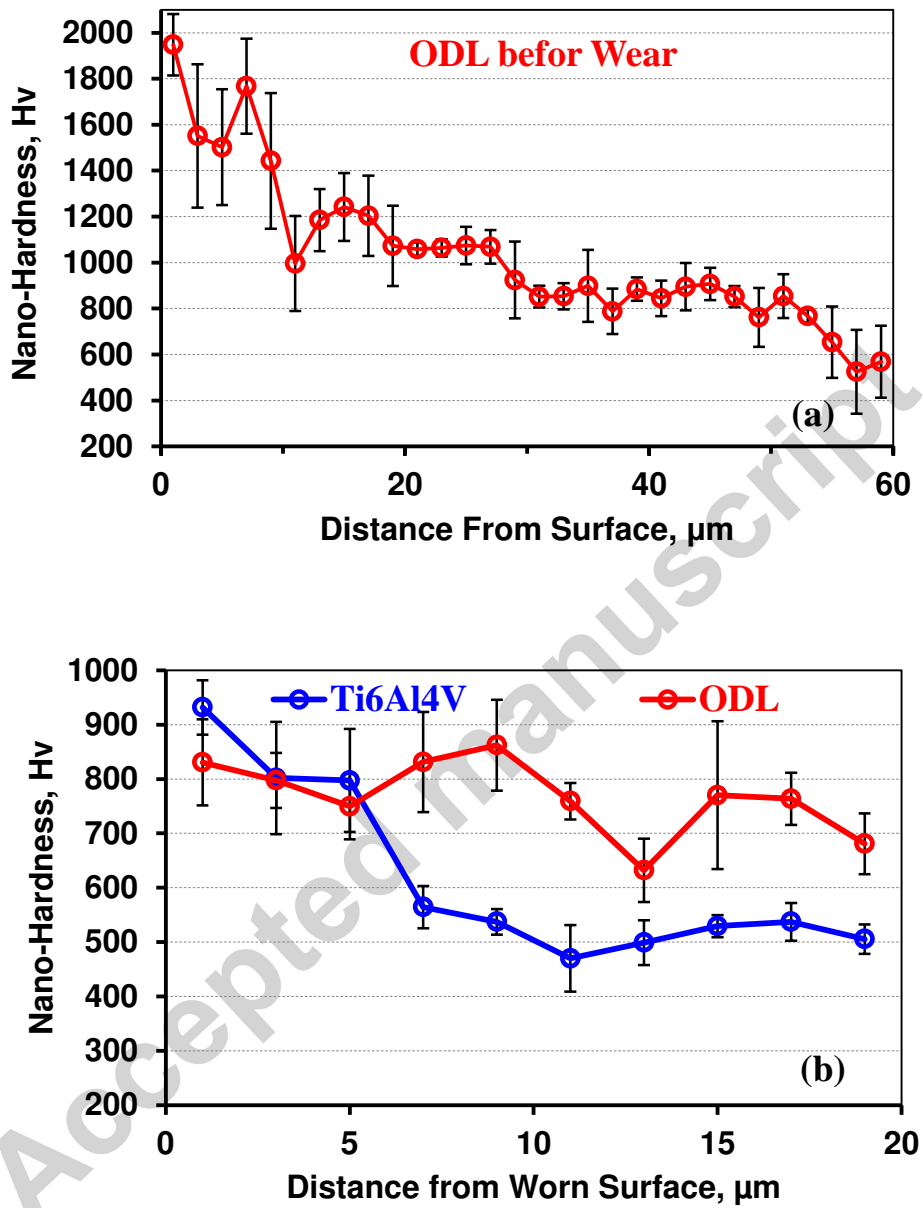
- [44] Y.T. Zhu, T.G. Langdon, Influence of grain size on deformation mechanisms: An extension to nanocrystalline materials, *Mater. Sci. Eng. A.* 409 (2005) 234–242. doi:10.1016/j.msea.2005.05.111.
- [45] X.D. Ren, W.F. Zhou, F.F. Liu, Y.P. Ren, S.Q. Yuan, N.F. Ren, et al., Microstructure evolution and grain refinement of Ti-6Al-4V alloy by laser shock processing, *Appl. Surf. Sci.* 363 (2016) 44–49. doi:10.1016/j.apsusc.2015.11.192.



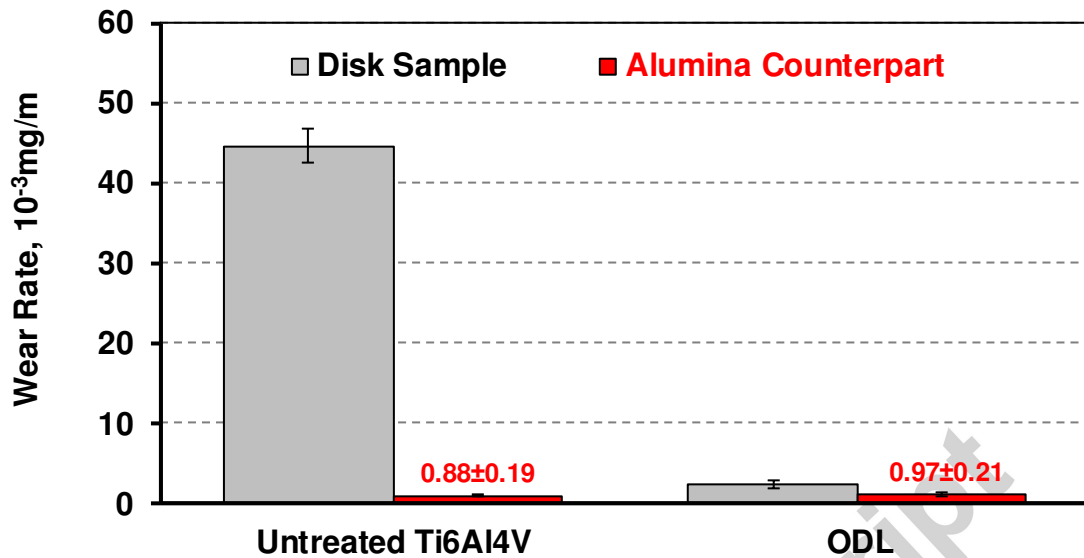
**Fig. 1.** Cell Viability of Ti6Al4V and the ODL samples after 24 h of cell culture. The data represent the mean value  $\pm$  standard deviation. All results are statistically equal.



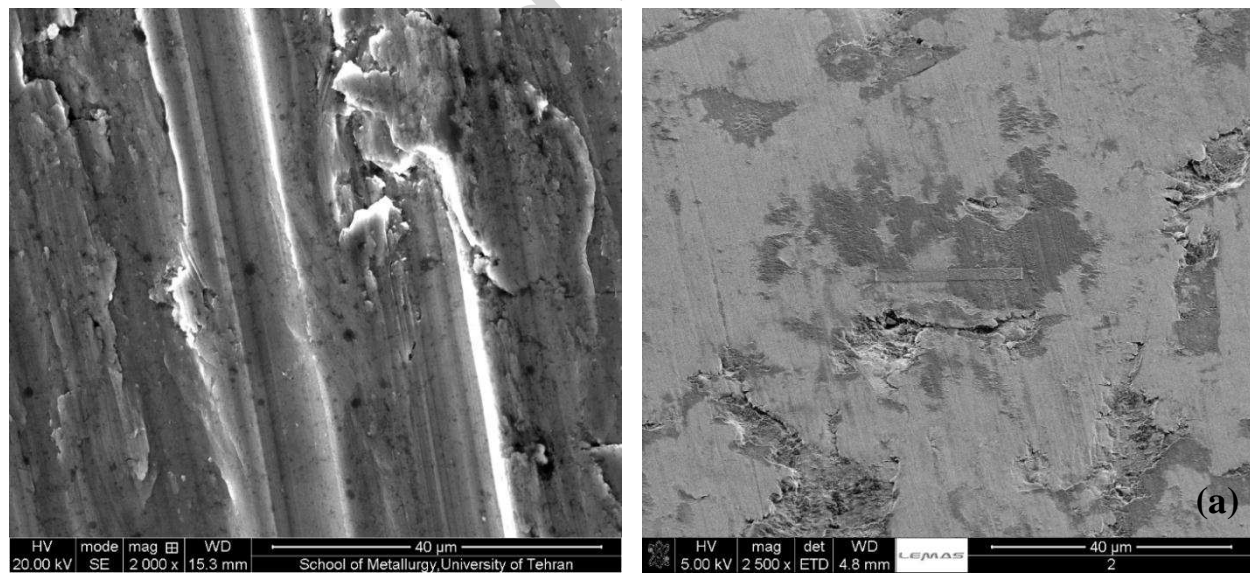
**Fig. 2.** Normal load versus penetration depth in the nano-indentation tests for Ti6Al4V and the ODL samples.



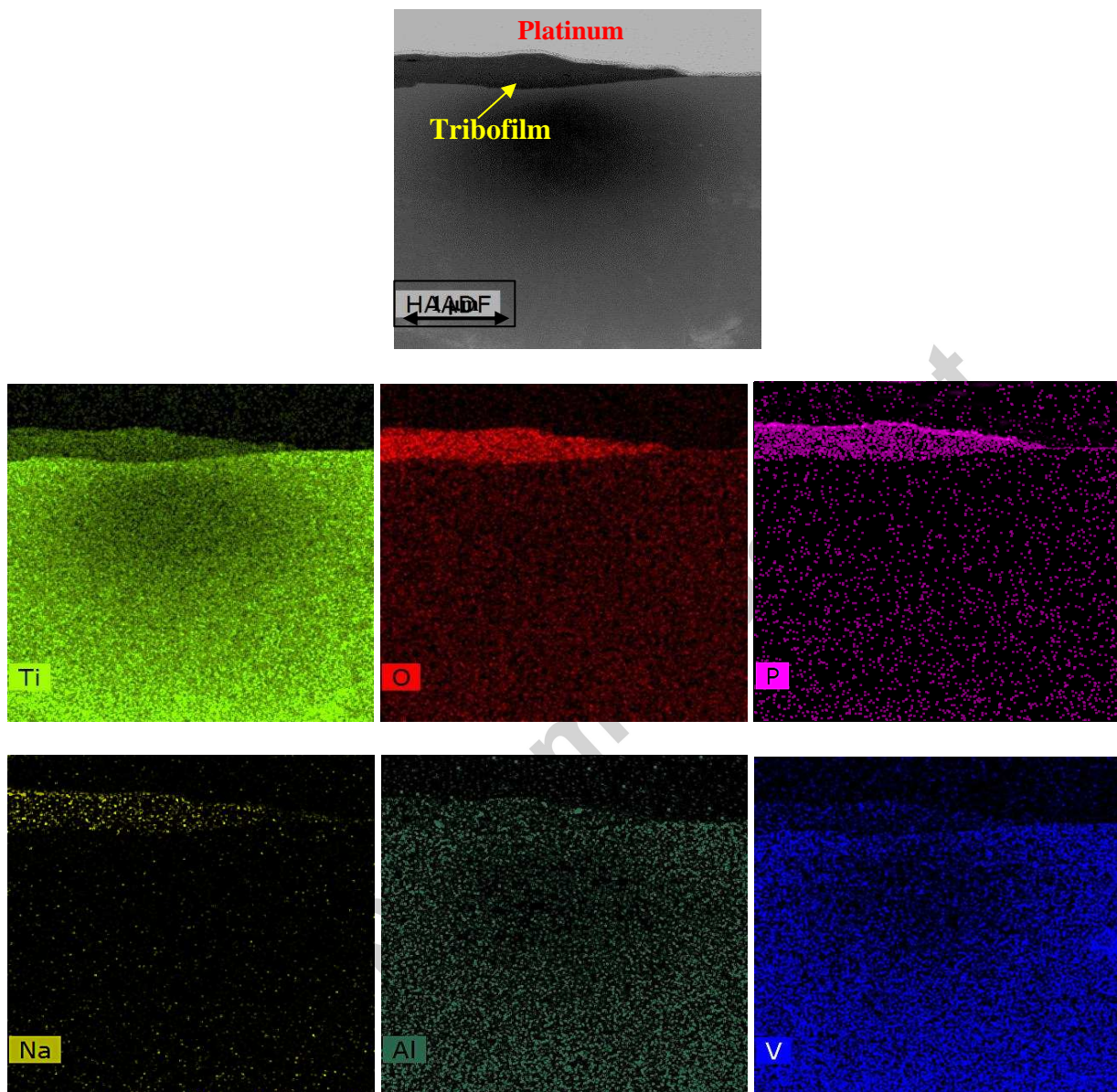
**Fig. 3.** Variation of hardness of the subsurface of; (a) the ODL sample before a wear test and (b) the wear tracks with distance from wear surfaces of the treated (ODL) and untreated (Ti6Al4V) samples.



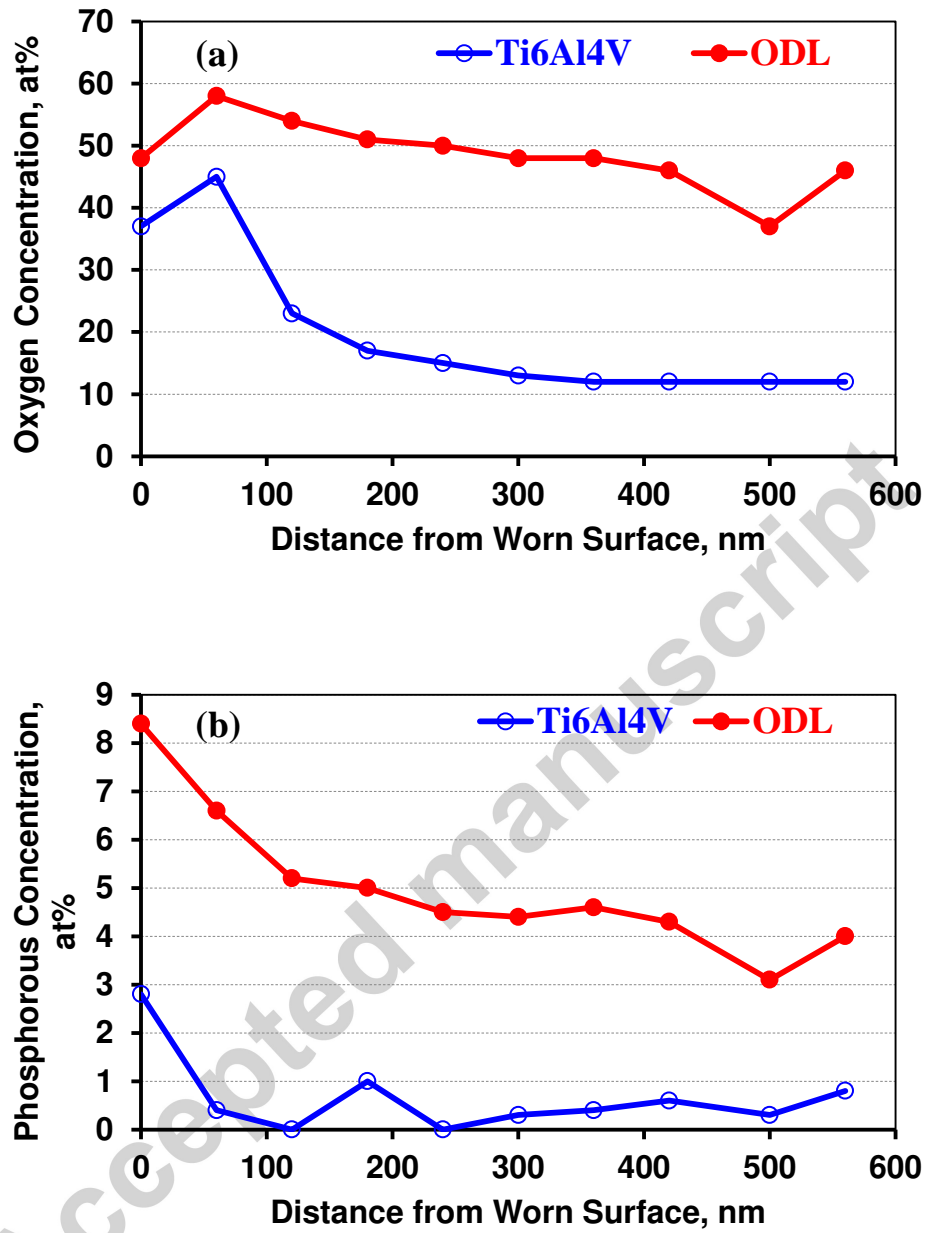
**Fig. 4.** Wear rates of Ti6Al4V, the ODL samples and the alumina counterparts under a normal load of 30 N at a sliding velocity of 0.1 m/s for a sliding distance of 1000 m.



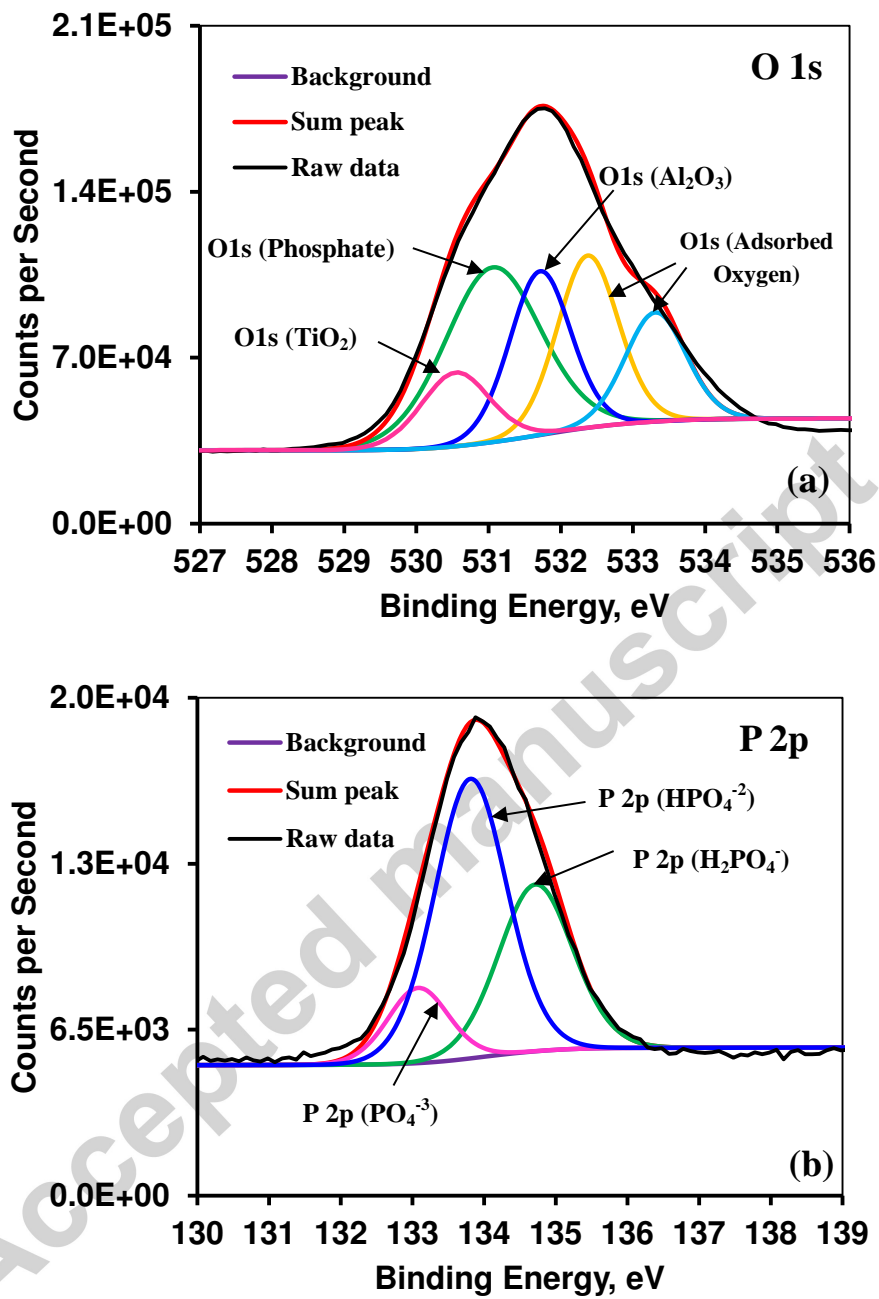
**Fig. 5.** SEM micrographs of the wear surfaces of: (a) untreated (Ti6Al4V) and (b) treated (ODL) samples under a normal load of 30 N, at a sliding velocity of 0.1 m/s for a sliding distance of 1000 m.

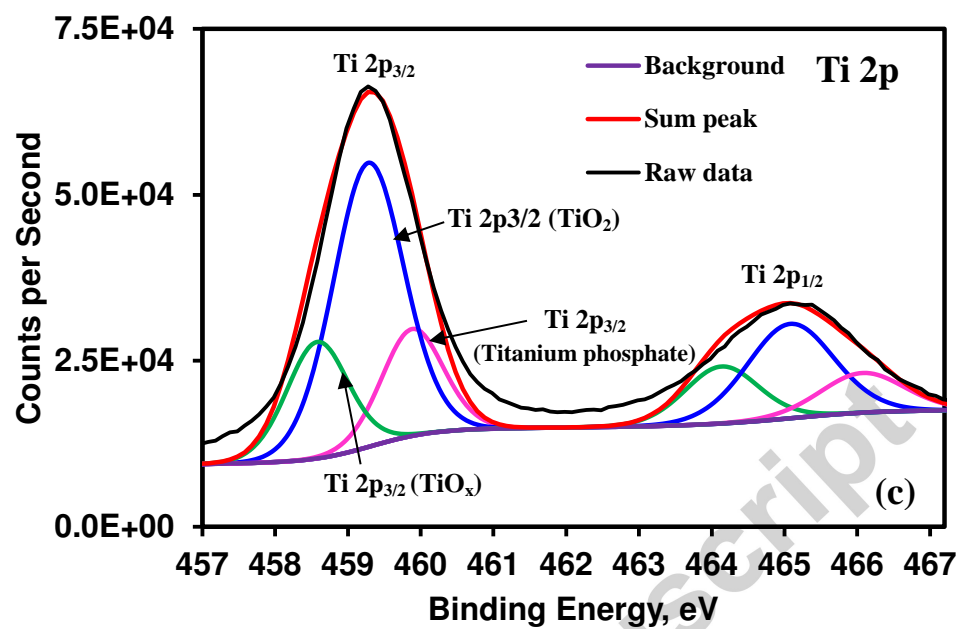


**Fig. 6.** STEM image of the cross section of the wear track of the ODL sample and EDS elemental maps of titanium, oxygen, phosphorous, sodium, aluminum and vanadium.

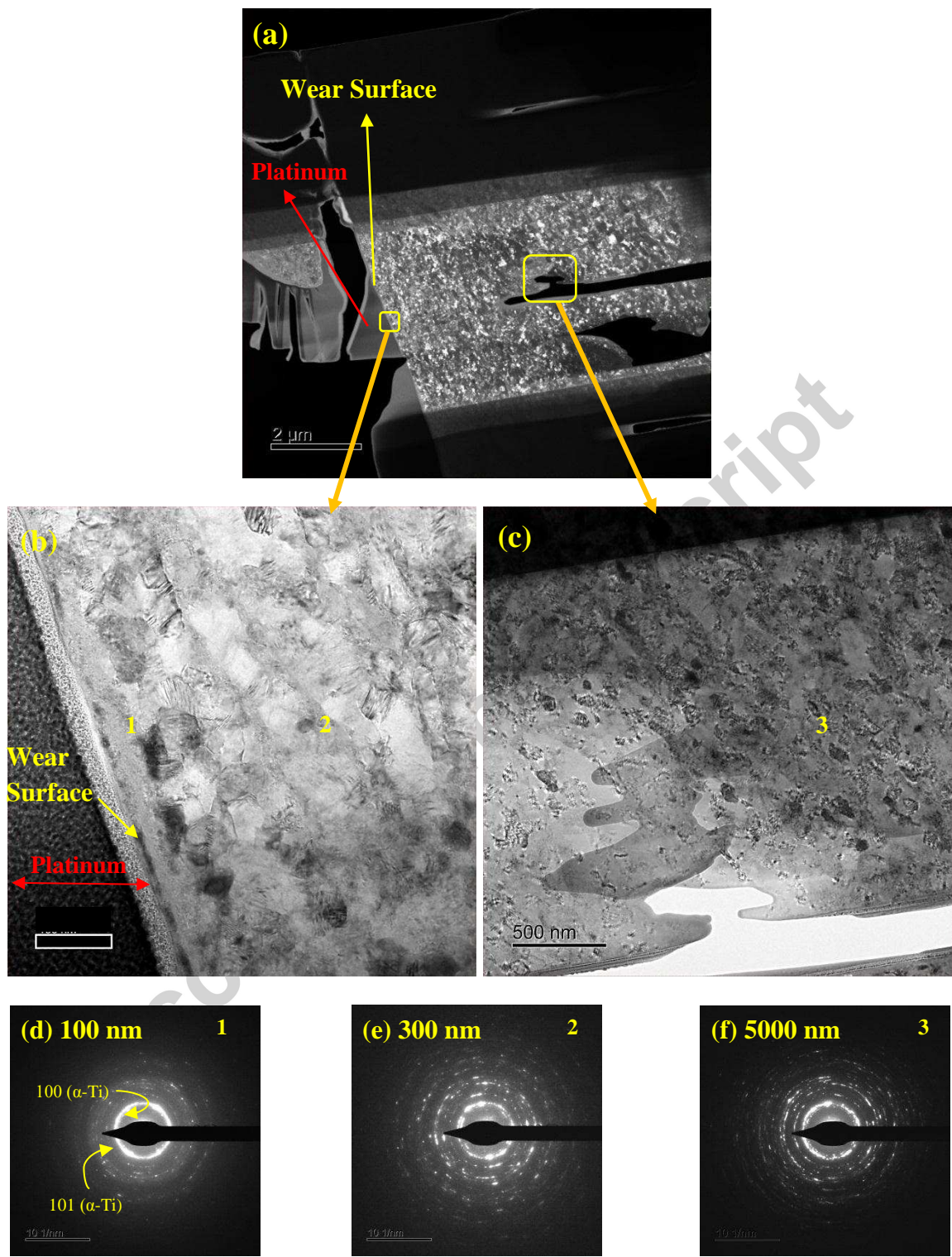


**Fig. 7.** Change in the concentration of: (a) oxygen and (b) phosphorous with distance from the wear surfaces of untreated (Ti6Al4V) and treated (ODL) samples obtained from XPS survey spectra of the various depths.

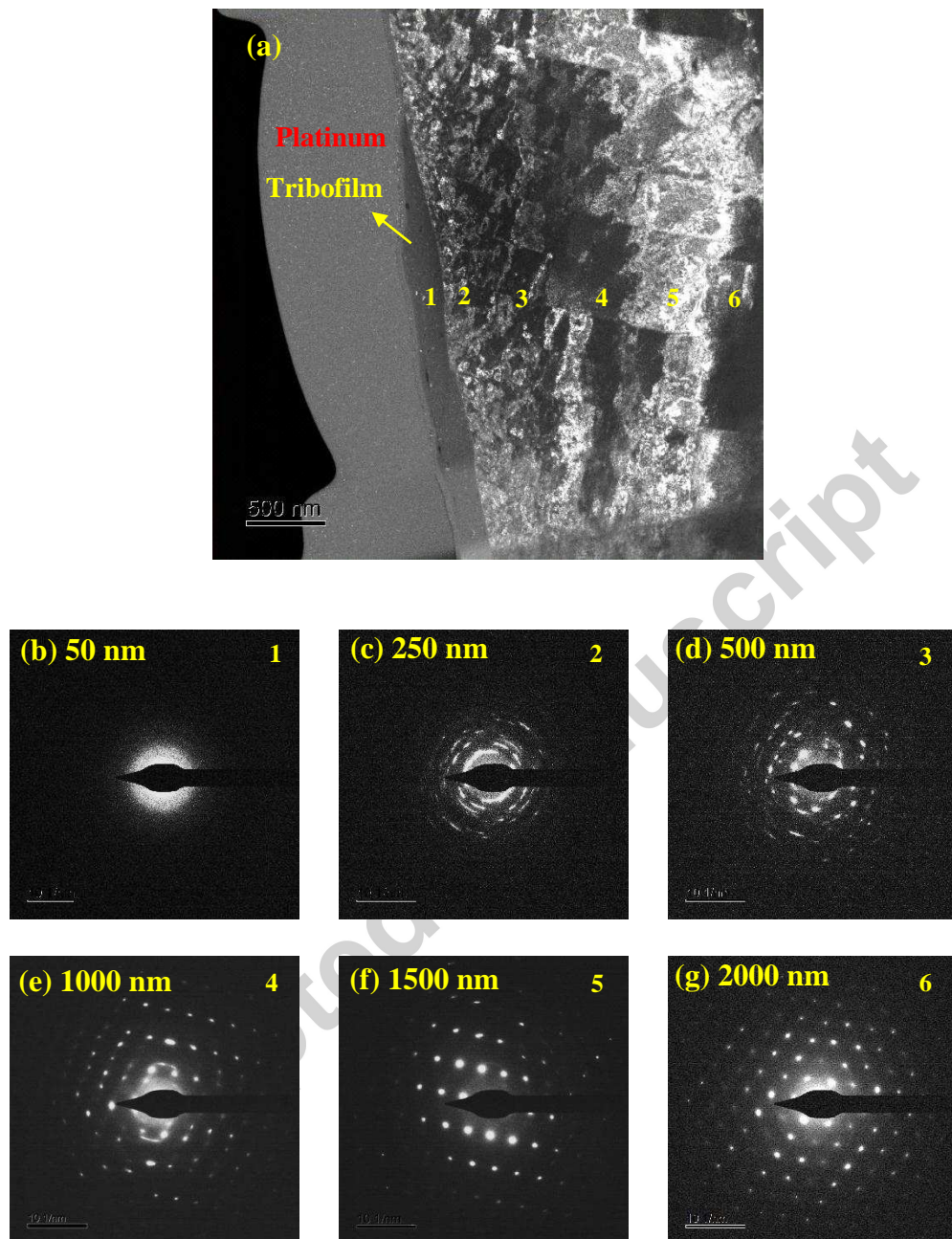




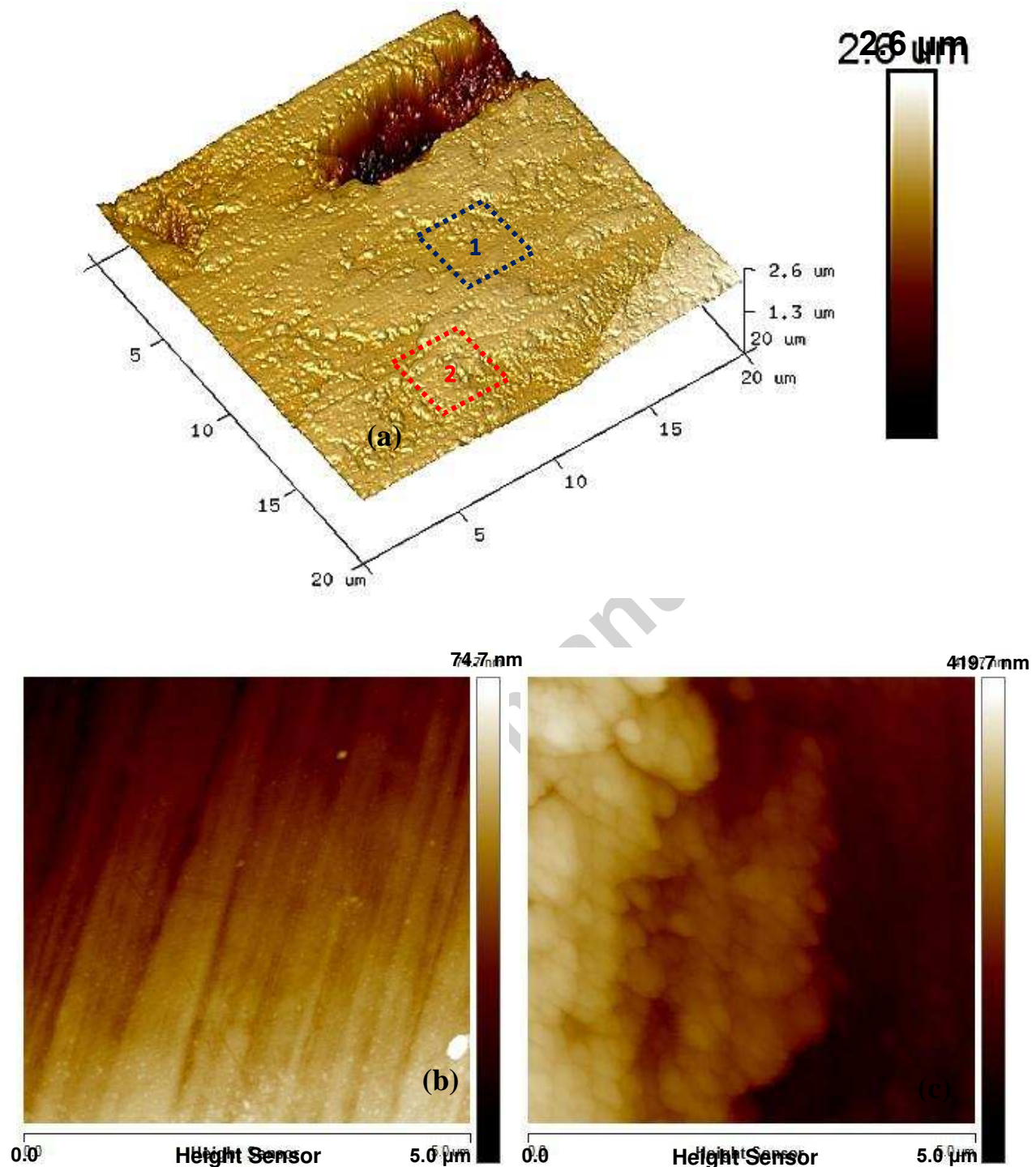
**Fig. 8.** High-resolution XPS spectra of: (a) O 1s; (b) P 2p and (c) Ti 2p form the tribofilm on the ODL.



**Fig. 9.** TEM images of the subsurface of Ti6Al4V sample worn in the simulated body fluid: (a) low magnification image; (b) and (c) higher magnification images; (d), (e), and (f) selected area electron diffraction of points 1 and 2 and 3 corresponding to the depths of 100 nm, 300 nm and 5000 nm from the wear surface, respectively.



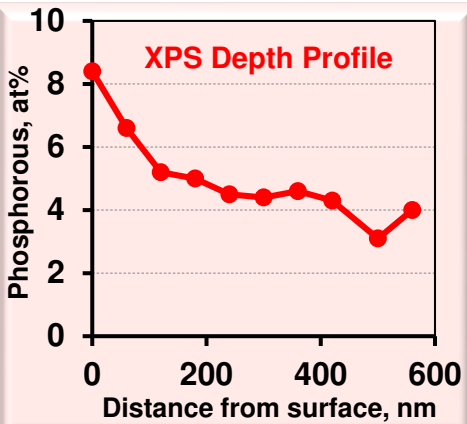
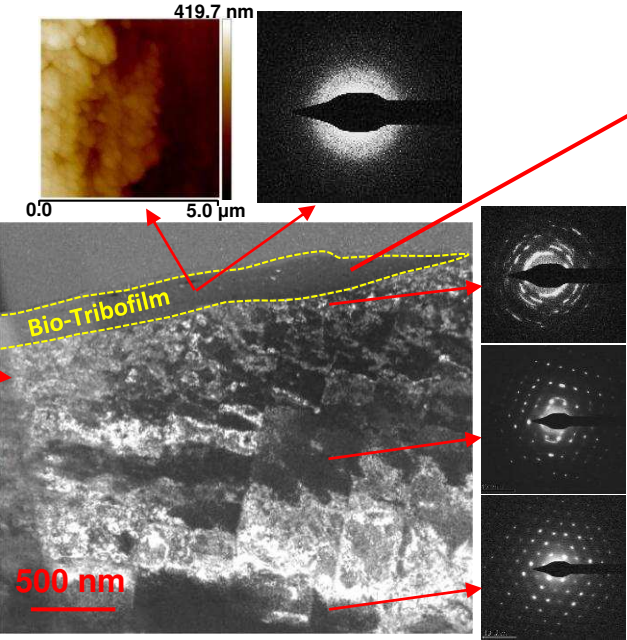
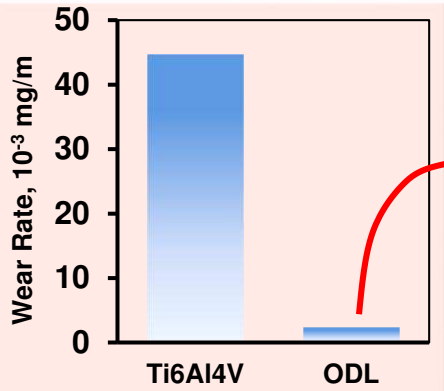
**Fig. 10.** (a) Dark-field TEM image of the cross section of the treated (ODL) sample worn in the simulated body fluid; (b)-(g) SAED patterns at various regions of the subsurface. Numbers in the upper right of SAED patterns indicate the points in Fig. 10a where patterns were obtained.



**Fig. 11.** AFM image of the wear track on the ODL sample: (a) 3D image of wear surface, and 2D images of (b) region 1 where no indication of the tribofilm is presented, and (c) region 2 showing the tribofilm.

## Highlights

- Oxygen diffusion in Ti6Al4V resulted in a higher hardness and a lower E/H ratio.
- Ti6Al4V and ODL samples indicated a similar cytocompatibility.
- A bio-tribofilm formation decreased the wear rate of ODL by about 95%.
- Nano-structured grains were formed in Ti6Al4V wear subsurface by high plastic flow.
- Low ability for plastic flow in ODL limited grain refinement of wear subsurface.



$\text{Al}_2\text{O}_3$ ,  $\text{TiO}_2$ ,  $\text{TiO}_x$ ,  
 $\text{HPO}_4^{2-}$ ,  $\text{H}_2\text{PO}_4^-$ ,  $\text{PO}_4^{3-}$ ,  
Titanium Phosphate,  
Adsorbed Oxygen